CFD SIMULATION OF FREE SURFACE FLOW AND HEAT TRANSFER OF LIQUID SLAG ON A SPINNING DISC FOR A NOVEL DRY SLAG GRANULATION PROCESS

Yuhua PAN[*], **Peter J. WITT and Dongsheng XIE**

CSIRO Minerals, Clayton, Victoria 3169, AUSTRALIA
[*]Corresponding author, E-mail address: Yuhua.Pan@csiro.au

ABSTRACT

A novel process for dry granulation of molten slag using a spinning disc is being developed by CSIRO. Molten slag is atomised by a spinning disc under centrifugal force and slag droplets are quenched and solidified via air to produce glassy granules and recover waste heat. In the present work, steady-state two-dimensional CFD simulations of fluid flow and heat transfer in the slag and the disc was carried out by using ANSYS CFX modelling package. The model domain is comprised of a solid disc, air and liquid slag before the slag film breaks up. Multiphase fluid flow and heat transfer were considered for the liquid slag with a free surface and the cooling air. The free surface was modelled with the continuum surface force method. Conjugate heat transfer between liquid slag and disc was included. The present model was applied to predict the thickness and temperature of the slag film prior to its rupture. Influences of factors including the pouring flowrate and temperature of liquid slag and the disc spinning rate on the slag film thickness and temperature were investigated.

Keywords: Spinning disc, granulation, simulation, modelling, CFD, free surface flow and heat transfer.

NOMENCLATURE

Alphabetic Symbols

C_μ constant in turbulence model
$\mathbf{C}_{\alpha\beta}$ interphase momentum transfer term
d diameter
$\mathbf{F}$ body force vector
F_1 first blending function in turbulence model
F_2 second blending function in turbulence model
$\mathbf{F}_s$ surface tension force vector
g gravitational acceleration
h specific enthalpy
k turbulence kinetic energy
Nu Nusselt number
p pressure
P_k production rate of turbulence kinetic energy
q heat flux
Q interphase heat transfer term
r volume fraction
Re Reynolds number
S strain rate
T temperature
$\mathbf{u}$ velocity vector
y^+ dimensionless distance

Greek Symbols

α heat transfer coefficient
α_1 constant in turbulence model
α_3 constant in turbulence model
β' constant in turbulence model
β_3 constant in turbulence model
δ_s surface-centred Dirac peak function
ε dissipation rate of turbulence kinetic energy
ε_b emissivity
φ_{spin} angular velocity of spinning disc
κ curvature of free surface
λ thermal conductivity
μ dynamic viscosity
μ_t turbulent viscosity
ρ density
σ Stefan-Boltzmann constant
$\sigma_{\omega 2}$ Prandtl number for ω in transformed k-ε model
$\sigma_{\omega 3}$ Prandtl number for ω in SST turbulence model
σ_{k3} Prandtl number for k in SST turbulence model
σ_s surface tension coefficient
ω turbulence eddy frequency

Common Subscripts:

α, β fluid phase identity (liquid slag or air)
a ambient
air bulk air
b boundary identity
ext external parameter
$film$ liquid slag film
$slag$ bulk slag
w wall

INTRODUCTION

Slags are high volume by-products or wastes from the iron and steel industry. For every tonne of hot metal produced, about 300 kg of blast furnace slags are produced. Each year, about two million tonnes of slags are produced in Australia. These slags are either air cooled or water granulated. Air cooled slags could be crushed and screened, and then used as road base materials. Water granulation is increasingly used to process molten blast furnace slags to produce glassy granules which could be used as cementitious materials for cement manufacture. These conventional slag processes, however, have some major short comings, from no heat recovery, air pollution, to consumption of a large amount of water.

Dry slag granulation using a spinning disc is emerging as an attractive alternative for slag processing. The

conception of dry granulation via a spinning disc was first proposed in 1980s. The recent work at CSIRO has led to a significant technology breakthrough in dry granulation process design by overcoming several major difficulties. Currently work is underway to extend the dry granulation process to incorporate heat recovery (Xie and Jahanshahi, 2008). The new integrated dry granulation and heat recovery process could be used for full recovery from the slag (to recover waste heat as high grade heat source and to produce glassy blast furnace slag granules for cement manufacture) and much reduced environmental impact (saving water and eliminating sulphur emission).

Slag granulation at a spinning disc involves complex fluid dynamics, phase transformation, and heat transfer. Molten slag is poured onto a spinning disc, spreads to become a liquid film, and eventually develops into a number of ligaments and breaks up into fine droplets under centrifugal forces (Figure 1). The fast motion is accompanied by simultaneous slag cooling due to heat transfer to the disc and surrounding air and the corresponding significant changes in slag properties such as viscosity and liquid to solid phase change. The situation is further complicated by inevitable fluctuation in slag tapping rate and temperature and variable operating parameters such as disc spinning rate.

Figure 1: Typical still image from high speed video recording of the dry granulation at a spinning disc in CSIRO dry slag granulation process.

In this work, CFD modelling techniques were applied to dry slag granulation via a metal spinning disc to gain valuable insights and deep understanding of the complex process. In particular, the formation of a solid freezing slag layer at the disc surface and spreading and formation of a liquid slag film have been studied as an aid for developing the optimal process design and for future scale-up of the process.

MODELLING PRINCIPLES

General Assumptions

The fluid flow phenomenon encountered for a liquid slag stream falling from the furnace crucible onto the disc, flowing and spreading across the disc is a typical free surface flow in which the two phases, liquid slag and air, are separated by a sharp interface or free surface. The phenomenon is further complicated by heat transfer from the slag to the disc and the solidification and formation of a thin solid slag layer that is in contact with the disc. Thus, conjugate heat transfer must be considered between the liquid slag region and the solid slag and disc. In order to

mathematically simulate these complex phenomena, the following general assumptions have been made:

- Continuous slag stream is poured from the crucible with a fixed temperature and mass flow or tapping rate;

- Steady-state fluid flow and heat transfer;

- A central and cylindrical slag stream such that is rotationally symmetric is assumed about the central axis of the stream and thus a two-dimensional computation domain can be applied;

- In the vicinity of the disc, the air flow is influenced only by the spinning disc and the motion of liquid slag;

- To reduce computational effort, only a part of the tapped slag stream and a limited portion of air near the disc are included in the computation domain;

- A constant Nusselt number is used to calculate heat exchange between liquid slag and air at the free surface; and

- A single temperature value, defined as slag "solidus", is adopted to judge the occurrence of solidification of the slag.

Governing Equations

In this work the liquid slag and air flow is modelled as a steady-state two-phase free surface flow problem with conjugate heat transfer to predict temperature within the disc and solid slag layer. Location of the liquid slag-air interface is determined by solving a pair of phase continuity equations given in Eqn. 1.

$$\nabla \cdot (r_\alpha \rho_\alpha \mathbf{u}_\alpha) = 0 \qquad (1)$$

As shown in Figure 1 the slag film eventually breaks into ligaments then droplets. To allow for this in future models separate velocity fields are obtained by solving a momentum Eqn. 2 for each phase.

$$\nabla \cdot [r_\alpha (\rho_\alpha \mathbf{u}_\alpha \mathbf{u}_\alpha)] = -r_\alpha \nabla p_\alpha \\ + \nabla \cdot [r_\alpha (\mu + \mu_t)(\nabla \mathbf{u}_\alpha + (\nabla \mathbf{u}_\alpha)^T)] + \mathbf{F}_\alpha + \mathbf{C}_{\alpha\beta} \qquad (2)$$

To account for surface tension at the free surface, $\mathbf{F}_\alpha$, is an additional momentum source that is approximated by using the Continuum Surface Force (CSF) method of Rackbill et al., 1992. This method transforms the surface force into a body force in the free surface layer. Interphase drag, $\mathbf{C}_{\alpha\beta}$, is calculated using a free surface model with the area derived from the volume fraction gradient assuming a Newtonian regime. To allow for convective and radiative heat transfer from the free surface separate energy equations are solved for the liquid and air phase according to Eqn. 3.

$$\nabla \cdot [r_\alpha (\rho_\alpha \mathbf{u}_\alpha h_\alpha)] = \nabla \cdot [r_\alpha (\lambda_{eff} \nabla T_\alpha)] + Q_\alpha \qquad (3)$$

Turbulent effects are accounted for by using the homogenous turbulence model, which is a phase weighted extension of the single phase Shear-Stress-Transport (SST) model. Eqns. 4 and 5 are solved to obtain the turbulent kinetic energy and turbulent eddy frequency.

$$\nabla \cdot (\rho \mathbf{u} k) = \nabla \cdot \left[\left(\mu + \frac{\mu_t}{\sigma_{k3}} \right) \nabla k \right] + P_k - \beta' \rho k \omega \qquad (4)$$

$$\nabla \cdot (\rho \mathbf{u} \omega) = \nabla \cdot \left[\left(\mu + \frac{\mu_t}{\sigma_{\omega 3}} \right) \nabla \omega \right] + (1 - F_1) 2 \rho \frac{\nabla k \nabla \omega}{\sigma_{\omega 2} \omega} \qquad (5)$$

$$+ \alpha_3 \frac{\omega}{k} P_k - \beta_3 \rho \omega^2$$

Further details of the constants and terms in the above equations are given in ANSYS (2009).

Disc Geometry and Computation Domain

The disc geometry is a flat cylinder of 50 mm diameter and 10 mm in height, as schematically illustrated in Figure 2(a). Figure 2(b) shows the two-dimensional computation domain covering half the disc, a layer of solid slag formed on the top face of the disc and a region enclosing parts of liquid slag and air above the solid slag layer. In the radial direction, due to rotational symmetry, the computation domain only extends from the axis to the side face of the disc.
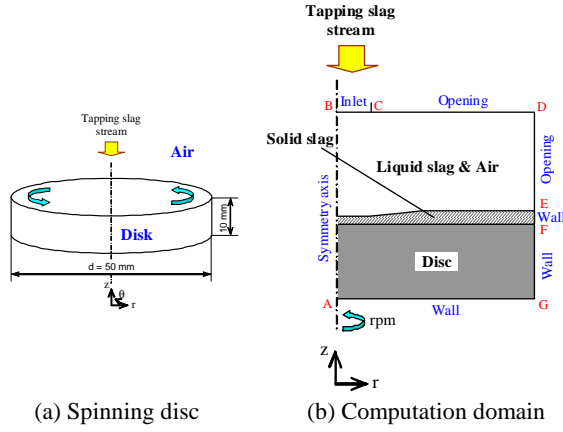

(a) Spinning disc (b) Computation domain

Figure 2: Schematic diagrams of three-dimensional disc geometry and two-dimensional computational domain.

In order to resolve the liquid slag layer and free surface, a fine mesh with an element size of 0.25 mm is employed in the vicinity above the interface between fluid and solid slag domains, and a five-layer inflation within the fluid domain is applied to this interface. This treatment has resulted in an average value of the dimensionless distance from the interface to the first nodal points in the fluid domain, y^+, to be around 0.1. This value implies that the turbulence model is integrated up to the interface and turbulent wall functions are not used in this region.

Boundary Conditions

In the computation domain shown in Figure 2(b), the boundaries are named and labelled in an alphabetical order, for which the specified conditions are given in Table 1.

Equation (6) in Table 1 is defined as,

$$T_{ext} = r_{slag} T_{film} + r_{air} T_{air} \qquad (6)$$

Boundary	Type	Condition
AB	Axis of symmetry	Zero fluxes
BC	Inlet	Liquid slag mass flowrate = Tapping rate Liquid slag temperature = Tapping temperature
CD & DE	Opening	External relative pressure = 0 Pa External temperature = Eq. (6)
EF & FG	Wall	Heat flux = Eq. (8)
GA	Wall	Temperature = Constant

Table 1: Boundary conditions.

where, T_{ext} is an external temperature only used when inflow occurs, for outflow a Neumann condition is used. T_{ext} depends on the local volume fraction of slag and air immediately passing the openings; T_{film} is the average temperature of the slag film just leaving the disc and assumed to be 1400 °C; T_{air} is the temperature of air surrounding the disc and assumed to be 1200 °C; and r_{slag} and r_{air} are, respectively, the volume fractions of liquid slag and air, which satisfy the following constraint:

$$r_{slag} + r_{air} = 1 \qquad (7)$$

The heat flux lost from the disc side face and the solid slag tip are estimated by using Eq. (8), which accounts for convection and radiation heat transfer:

$$q_b = -\alpha_b (T_b - T_a) - \varepsilon_b \sigma (T_b^4 - T_w^4) \qquad (8)$$

where, T_b is the temperature of the disc side face or solid slag tip face; T_a is the bulk air temperature; T_w is the enclosure wall temperature; ε_b is the emissivity of disc or solid slag, σ is the Stefan-Boltzmann constant; and α_b is the boundary heat transfer coefficient, which is estimated by using the published empirical dimensionless correlation for rotating cylindrical surfaces from Etemad (1955),

$$h_b = \frac{\lambda_{air}}{d_b} Nu_b \qquad (9)$$

$$Nu_b = 0.076 \mathrm{Re}_b^{0.7} \qquad (10)$$

and

$$\mathrm{Re}_b = \frac{\rho_{air} \varphi_{spin} d_b^2}{2 \mu_{air}} \qquad (11)$$

The definition of the symbols involved in all the above-mentioned equations is given in the Nomenclature.

Material Properties

Table 2 gives the thermophysical properties of liquid slag, solid slag, disc and air used in the present modelling work.

Material	Density (kg/m³)	Dynamic viscosity (Pa·s)	Thermal conductivity (W/mK)
Liquid slag[1]	2590[a]	0.7[b]	Eq. (12)[c]
Solid slag[1]	3100[d]	-	Eqs. (12) & (13)[c]
Stainless steel disc[2]	8000	-	17.6
Air[3]	1.185	Eq. (14)	Eq. (15)

[1]a: Inaba et al. (2004), b: Purwanto et al. (2005), c: Nagata and Goto (1984), d: Measured
[2]http://www.azom.com/details.asp?ArticleID=863
[3]http://users.wpi.edu/~ierardi/FireTools/air_prop.html

Table 2: Material thermophysical properties.

The equations mentioned in Table 2 are given by the following expressions:

$$\lambda_{slag} = -99.552 + 0.19672 T_{slag} - 1.2574 \times 10^{-4} T_{slag}^2$$
$$+ 2.625 \times 10^{-8} T_{slag}^3$$
$$\text{(for } T_{slag} \geq 1373.15 \text{ K)} \quad (12)$$

$$\lambda_{slag} = 0.7095 + 7.3468 \times 10^{-4} T_{slag} + 7.6683 \times 10^{-7} T_{slag}^2$$
$$- 6.5718 \times 10^{-10} T_{slag}^3$$
$$\text{(for } T_{slag} < 1373.15 \text{ K)} \quad (13)$$

$$\mu_{air} = 1.0 \times 10^{-6} (-\frac{2573.46}{T_{air}} + 18.3796$$
$$+ 0.029247 T_{air} - 3.4702 \times 10^{-6} T_{air}^2) \quad (14)$$

$$\lambda_{air} = 0.00318 + 8.616 \times 10^{-5} T_{air}$$
$$- 3.203 \times 10^{-8} T_{air}^2 + 6.214 \times 10^{-12} T_{air}^3 \quad (15)$$

In addition, the slag "solidus" is estimated to be 1388 °C, which is used to judge the occurrence of solidification according to the model predicted temperature field. The surface tension coefficient of liquid blast furnace slag is taken as 0.478 N/m (Inaba et al., 2004). A value of 600 is set for the Nusselt number at free surface to account for heat exchange between liquid slag and air.

Solution Method

The governing equations expressed by Eqs. (1) through (5) together with the boundary conditions given in Table 1 were solved numerically using the commercial CFD package ANSYS/CFX 11 (ANSYS Inc., 2009).

Solidification of liquid slag into solid slag was treated by using a trial and error method. With this method, we first start the simulations with a predefined solid slag region in the computation domain and then intermittently adjust the geometry of this region to follow the position of the slag "solidus" isotherm in the numerical results. In this way, and after a few iterations of adjusting the shape of this region, the solid slag profile becomes consistent with the slag "solidus" isotherm, such that the solid slag layer profile and thickness can be predicted. Furthermore, as a means of model validation, the predicted solid slag layer thickness was compared with that measured in number of granulation experiments. The model validation results will be described in the following section.

RESULTS AND DISCUSSION

Typical Modelling Results

Prediction of free surface profile

One of the important objectives of the CFD model as applied in the present work is to predict the free surface profile of liquid slag. From the free surface one can further predict the thickness of the slag film at the disc circumference prior to it rupturing into droplets. As an example, Figure 3 shows the predicted free surface profile indicated by the border between the red colour region (liquid slag) and the blue colour region (air). Under the operating condition shown in the figure, the model predicts that the slag film thickness close to the disc edge is 0.86 mm.

Prediction of temperature fields

Figure 4 depicts the model predicted temperature distribution in liquid slag, solid slag, disc and air near the centre of the rotating disc. Under the operating condition indicated in the figure, the model predicts that the average temperature of the liquid slag film at the exit of the computation domain is 1446.8 °C. Knowledge about this temperature is crucial for controlling film properties, such as viscosity and surface tension, as these are strong functions of temperature and control slag granule formation.
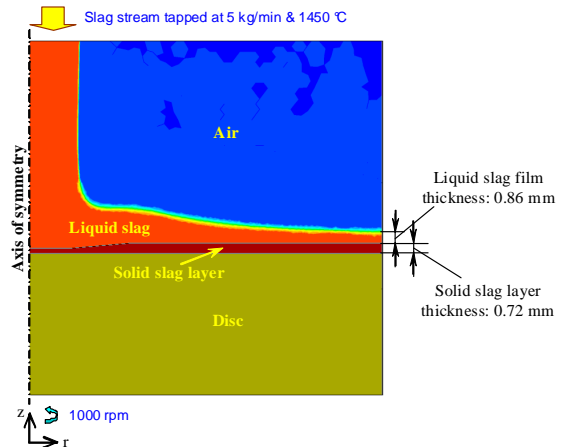

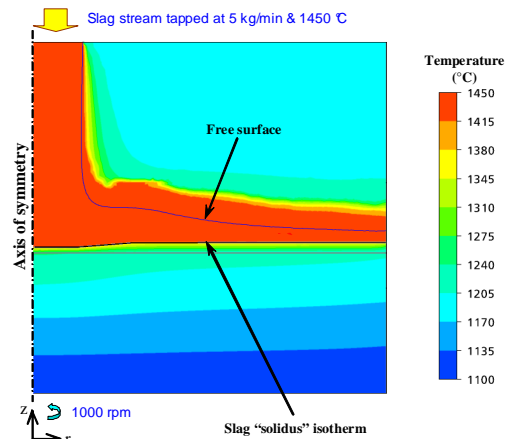**Figure 3**: Predicted liquid slag free surface profile.

Figure 4: Predicted temperature fields.

Prediction of flow fields

The model predicted liquid slag and air flow fields are shown in Figure 5. This figure depicts the strong downward flow of the tapping stream and that in the vicinity of the free surface both the slag and the air flow have high velocities. Away from the slag film, the air flow decays rapidly. A careful examination on the slag film region reveals that the radial velocity of liquid slag also decreases in the direction towards the solid slag layer. This is due to the wall and boundary layer effect of the solid slag.

Prediction solid slag profile

Figures 3 to 5 depict the profile of the solid slag layer predicted by the model (i.e., the slag "solidus" isotherm). As seen from these figures, the thickness of the solid slag layer is nearly uniform across a major part of the disc's top face, except for the centre zone impinged by the tapping liquid slag stream where a thinner solid slag layer exists.

4

Under the operating condition indicated in Figure 3, the model predicted thickness of the solid slag layer close to the disc edge is 0.72 mm.
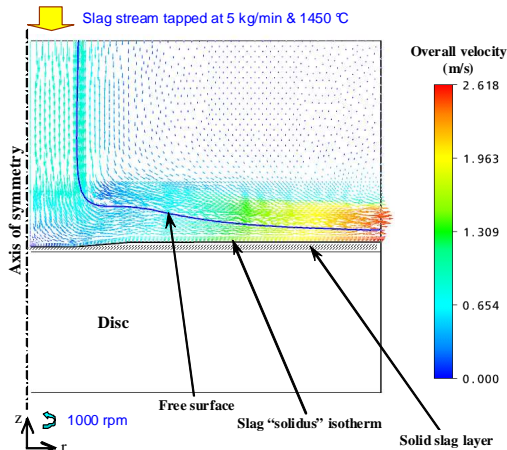

Figure 5: Predicted liquid slag and air flow fields.

Model Validation

The complexity of the fluid flow and heat transfer phenomena occurring on a spinning disc makes it very hard to facilitate reliable measurements of the velocity or temperature of the fast moving and rotating materials. Therefore, it is difficult to validate the CFD model by measuring velocity and/or temperature in experiments. Instead we were able to use the thickness of the solid slag layer deposited on the disc's top face during the granulation experiments to indirectly validate our model. Figure 6 shows a comparison of the predicted solid slag layer thickness with that measured at two different radial positions on the disc's top face (about one- and two-thirds away from the centre, respectively) for three experimental runs under the operating conditions given in the figure. It can be seen from Figure 6 that the model gives predictions of solid slag layer thickness that are generally in good agreement with the measurements (only with slight overestimations).

The validation results shown in Figure 6 provide a level of confidence that the CFD model is able to predict the heat transfer and frozen slag layer and thus can be used for investigating the flow and heat transfer phenomena taking place on a spinning disc. Further validation by using solid slag layer thickness measured from more granulation experiments and by measuring other parameters can be used to improve the validity of the model.
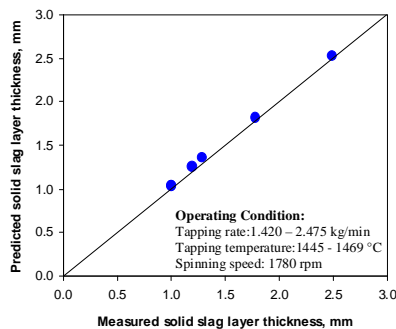

Figure 6: Comparison between predicted solid slag layer thickness and the measurements.

In all subsequent simulations the solid slag profile is adjusted to follow the position of the slag "solidus" isotherm. In this way, the CFD model is able to account for the slag solidification phenomena and thus can be applied to investigate the influences of operating conditions on the key parameters, such as slag film thickness and temperature, for the dry slag granulation process.

Influences of Operating Parameters on Slag Film Thickness and Temperature

To gain an understanding of the sensitivity of solid layer thickness, liquid slag film thickness and the film temperature on operating parameters a series of simulations looking at changes in operating parameters has been performed.

Influence of slag tapping rate

From the present modelling investigation, it was found that the slag tapping rate has a major influence on the liquid slag film thickness, as shown in Figure 7. It can be seen from this figure that increasing the tapping rate results in a thicker slag film thickness at the edge of the disc. For instance, an increase in the tapping rate from 2 to 8 kg/min leads to an increase in film thickness by about 0.4 mm. Figure 8 shows the influence of tapping rate on slag film temperature. It can see from this figure that the effect of tapping rate on the slag film temperature is very limited, with a few degrees increase. This is because, with the high spinning of the disc, liquid slag on the disc has a high velocity and thus has a short residence time on the disc, resulting in limited heat losses to the disc and air.
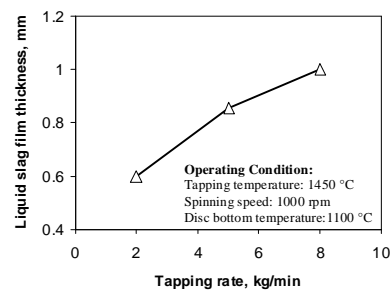

Figure 7: Influence of tapping rate on film thickness.

Influence of slag tapping temperature

The most dominant influence of slag tapping temperature is on the slag film temperature, which is illustrated in Figure 9. It can be seen from this figure that the relationship between the tapping temperature and the film temperature is quite linear and the latter is only a few degrees (2.5 to 4 °C) lower than the former.

Influence of disc spinning speed

The most obvious influence of spinning speed is found on the slag film thickness, as depicted by Figure 10. We can see from this figure that an increase in disc spinning speed from 1000 to 2000 RPM leads to a decrease in the film thickness by about 0.35 mm.
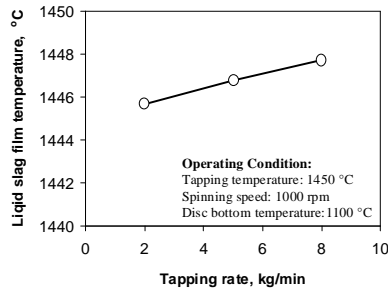
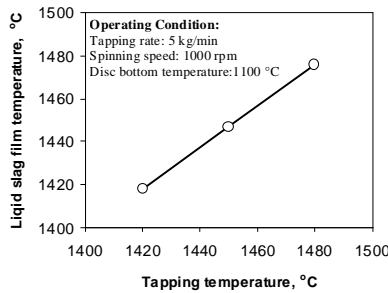**Figure 8**: Influence of tapping rate on film temperature.

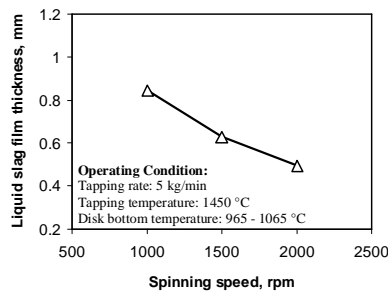**Figure 9**: Influence of tapping temperature on film temperature.

Figure 10: Influence of spinning speed on film thickness.

As a summary, the above-mentioned modelling results demonstrate that the slag film thickness can be effectively controlled by adjusting the slag tapping rate and disc spinning speed, whereas the slag film temperature can be more directly controlled by adjusting the slag tapping temperature. Therefore, by appropriate selection of these operating parameters slag film properties can be controlled to achieve favourable conditions for disintegration of the slag film into desired droplets and final granules.

CONCLUSION

Steady-state two-dimensional CFD modelling studies have been carried out to simulate fluid flow, heat transfer and solidification of liquid blast furnace slag on a spinning disc for dry granulation of slag. The model is capable of predicting the liquid slag free surface profile, the flow and temperature fields and the solid slag layer thickness. The most important outputs from the model are predictions of the thickness and temperature of liquid slag film before it leaves the disc and ruptures, which can be used to deduce the formation of slag droplets/granules. For the spinning disc with the geometry investigated in this work, the modelling results indicate that, i) the slag film thickness can be effectively controlled by adjusting slag tapping rate and disc spinning speed; ii) an increase in tapping rate from 2 to 8 kg/min leads to an increase in the film thickness by about 0.4 mm; iii) an increase in disc spinning speed from 1000 to 2000 RPM results in a decrease of slag film thickness by about 0.35 mm; iv) the slag film temperature can be directly controlled by adjusting the slag tapping temperature, with the former being nearly linearly dependent on the latter. Appropriate controls on tapping rate, tapping temperature and spinning speed will maintain a slag film with properties favourable for producing desired slag granules.

ACKNOWLOGMENT

REFERENCES

ANSYS Inc., 2009, ANSYS CFX User Manual, Release 12.0.

BACKBILL, J.M.; KOTHE, D.B. and ZEMACH, C., (1992), "A continuum method for modelling surface tension", *J. Computational Physics*, **100**, 335-354.

Etemad, G.A., (1955), "Free Convection Heat Transfer from a Rotating Cylinder to Ambient Air, with Interferometric Study of Flow", *Trans. ASME* **77**, 1283-1289.

INABA, S.; KIMURA, Y.; SHIBATA, H. and OHTA, H., (2004), "Measurement of physical properties of slag formed around the raceway in the working blast furnace", *ISIJ International*, **44**, No. 12, 2120-2126.

NAGATA, K. and GOTO, K.S., (1984), "Heat conductivity and mean free path of phonons in metallurgical slags", *Proc. Second Int. Symp. on Metallurgical Slags and Fluxes*, Edited by Fine, H.A. and GASKELL, D.R., The Metallurgical Society of AIME, Lake Tahoe, Nevada, USA, November 11-14, 875-889.

PURWANTO, H.; MIZUOCHI T. and Akiyama T., (2005), *Materials Transactions*, **46**, No. 6, 1324-1330.

XIE, D. and JAHANSHAHI, S., (2008), "Waste Heat Recovery from Molten Slags", International Congress on Steel 2008 (ICS2008), 6-8 October 2008, Gifu, Japan.